Journal Pre-proof

Thermoluminescence characterization of natural and synthetic irradiated Ce-monazites

V. Correcher, C. Boronat, J. Garcia-Guinea, J.F. Benavente, T. Rivera-Montalvo

PII: S1002-0721(23)00042-X

DOI: https://doi.org/10.1016/j.jre.2023.02.012

Reference: JRE 1412

To appear in: *Journal of Rare Earths*

Received Date: 28 November 2022

Revised Date: 11 January 2023

Accepted Date: 9 February 2023

Please cite this article as: Correcher V, Boronat C, Garcia-Guinea J, Benavente JF, Rivera-Montalvo T, Thermoluminescence characterization of natural and synthetic irradiated Ce-monazites, *Journal of Rare Earths* (2023), doi: https://doi.org/10.1016/j.jre.2023.02.012.

This is a PDF file of an article that has undergone enhancements after acceptance, such as the addition of a cover page and metadata, and formatting for readability, but it is not yet the definitive version of record. This version will undergo additional copyediting, typesetting and review before it is published in its final form, but we are providing this version to give early visibility of the article. Please note that, during the production process, errors may be discovered which could affect the content, and all legal disclaimers that apply to the journal pertain.

© 2023 Published by Elsevier B.V. on behalf of Chinese Society of Rare Earths.

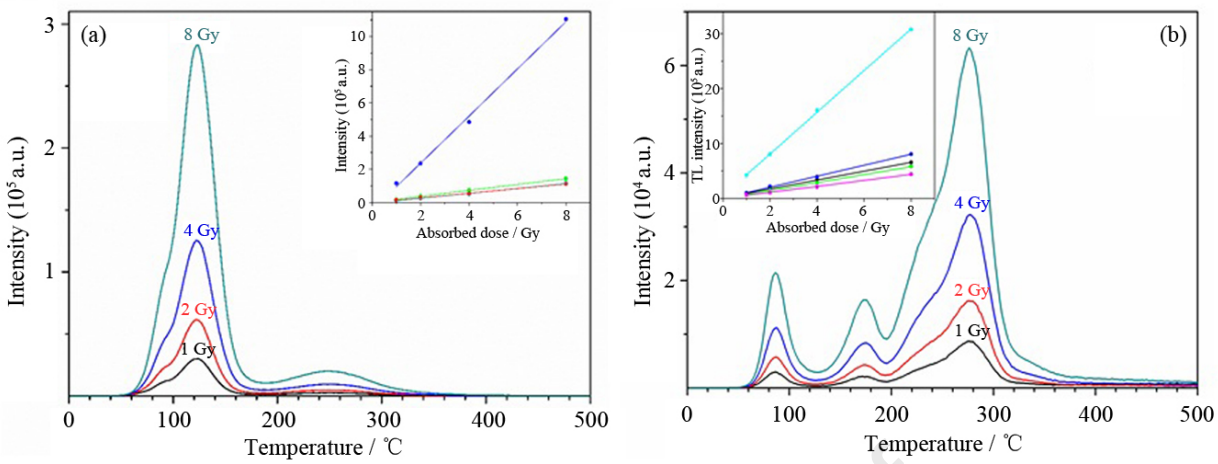

Journal Pre-proof

Journal Pre-proof

Thermoluminescence characterization of natural and synthetic irradiated Ce-monazites

V. Correcher[a]*, C. Boronat[a], J. Garcia-Guinea[b], J.F. Benavente[a], T. Rivera-Montalvo[c]

[a]*CIEMAT, Av. Complutense 40, 28040 Madrid, Spain*

[b]*MNCN-CSIC, J. Gutierrez Abascal 2, 28006 Madrid, Spain*

[c]*Instituto Politécnico Nacional, CICATA-IPN, Av. Legaria 694, México City 11500, Mexico*

**Corresponding author. E-mail address: v.correcher@ciemat.es*

Abstract

The thermoluminescence (TL) emission of synthetic and natural Ce-monazites was characterized here to determine the potential application in the identification of microscopic defects from a qualitative point of view trying to link each TL peak to a chemical-physical process. The kinetic parameters that lead the luminescence processes were calculated by means of variable heating rate and computing glow curve deconvolution methods and allow identifying three groups of components at ~90, 130 and 290 ºC (for the mineral sample) and ~90, 170, 220, 270 and 320 ºC (for the synthetic $CePO_4$:$Nd_{0.20}$,$La_{0.25}$). The main differences appreciated in these complex TL curves are mainly due to (i) the content of impurities (natural sample contains lanthanides as well as U 0.60% and Th 5.22%) and (ii) the degree of crystallinity of the samples which is directly related to the type of impurities (synthetic monazite relies only on Nd and La). The behavior of the dose response in the range of 1–8 Gy is similar for both samples; the TL intensity increases linearly as the dose increases without changes in the position of the maxima, denoting first-order kinetic luminescence mechanism. Each peak could be mostly associated with structural defects (i.e. phase transitions), chemical reactions (i.e. $Ce^{3+} \leftrightarrows Ce^{4+}$ redox reaction, dehydration or dehydroxylation processes) or intrinsic defects (i.e. Frenkel defects, ODCs or NBOHCs).

Keywords: Thermoluminescence; kinetic parameters; Phosphate; Ce-monazite; Defects; Rare earths

1. Introduction

Phosphates in general and lanthanide phosphates ($LnPO_4$, for instance, monazite or xenotime) in particular, are of especial interest in the field of nuclear science technology since and can be employed as potential long-term storage of some actinides including Pu or high-level radioactive wastes (i.e. fission-product rare earths)[1]. Monazite appears to be a suitable material for such purposes since (i) it is able to host significant amounts of rare earth elements (REEs), (ii) exposure to radiation can induce partial amorphization that is reversible, (iii) it displays a negative temperature coefficient of solubility; solubility decreases as temperature increases and (iv) it exhibits high chemical stability[2]. These materials also display luminescence properties that make them suitable compounds to be used as plasma display panels[3], ionic conductors, phosphors and VUV scintillators[4] and photon convertors for solar cells[5], due to its physical and chemical properties, optical emissivity, high resistance to corrosion or radiation damage. Natural monazites, that are usually formed due to the transformation of apatites or metapelite rocks by hydrothermal fluids, are also the main ore for Th extraction and a secondary source of U after uraninite (UO_2) or coffinite $U(SiO_4)_{1-x}(OH)_{4x}$[6].

$LnPO_4$ (Ln: La, Ce, Nd, Pr, Sm, Eu, Gd, Tb), which are easily synthesized by hydrothermal, solid state, mechano- and pyrochemical methods, etc., display two complex crystalline structures: hexagonal lattice with D_{6h} symmetry (rhabdophane, $LnPO_4 \cdot xH_2O$ (x= 0.3–0.7)) and monoclinic lattice with C_{2h} symmetry (monazite, $LnPO_4$)[7]. Monazite structure (space group $P2_1/n$) consists of an irregular nine-fold coordination Ln site polyhedral (where Ce–O bond lengths differ among them; one of them is a longer bond 0.278 nm length with respect to the others 0.253 nm) linked to distorted PO_4 tetrahedra 8 [8,9]. Additionally, the four P–O bonds differ in the lengths from ~1.53 to 1.546 nm[10] where the O is coordinated to one P and two Ln atoms giving rise to chains of LnO_9-PO_4 sharing O–O edges along the c-axis[11]. Nevertheless, the Ln–O bond distances decrease as the atomic number increases attending to the well-known 4f REEs series contraction. Thus, the unit-cell parameters differ among different samples by 0.00263, 0.00353 and 0.0011 nm respectively for a, b and c axes and for $CePO_4$ samples; β angle varies linearly with the volume depending on the Ln (Sm, Pr, Ce or La) placed in the PO_4 lattice[11]. Consequently, one can guess that the lattice allows hosting dopants giving rise to point and structural defects in the lattice[7,12]. Such defects (intrinsic: Schottky, Frenkel defects; extrinsic: dopants; structural: phase transitions or stacking fault defects, etc.; or chemical due to dehydration, dehydroxylation, damage from ionizing self-irradiation, usually observed in natural monazites or redox reactions), defined as any chemical-structural change that modifies a regular pattern, will act as electrons and holes traps inducing luminescence processes (thermoluminescence (TL), cathodoluminescence, etc.). The position of the glow peak is associated with a specific defect although, for example, slight variations in the order of crystallinity of the lattice structure can give rise to subtle changes in the position of the

wavebands and their intensities[13]. In the case of the TL emission, the mechanism where the electrons release the traps to recombine with the holes with the corresponding photon emission, will be led by the kinetic parameters linked to the aforementioned defects: activation energy (*E*), frequency factor (*s*) and order of kinetics (*b*) that can be calculated by different methods attending to the complexity of the experimental glow curve. Thus, isothermal decay or phosphorescence decay[14], peak shape[15], initial rise[16], variable heating rate (VHR)[17] or computerized glow curve deconvolution (CGCD)[18] appear as the more acceptable tools for the TL glow curve analysis. More recently, a more simple methodology has been described to analyze TL glow curves assuming arbitrary recombination-retrapping rates[19].

This work focuses on the calculation of the TL kinetic parameters from the glow emission of a synthetic ($CePO_4$:$La_{0.25}Nd_{0.20}$) and the natural analogue monazite containing significant amounts of lanthanides using both CGCD and VHR methods. The differences and similarities observed can allow us to discern the groups of components specifically linked to intrinsic and structural defects, as well as defects induced by chemical reactions in both natural and synthetic Ce-monazite samples. As far as we know, the novelty of this work lies in the fact that there are no previous studies on the microscopic defects in Ce-monazite (natural and synthetic) irradiated at low doses (up to 8 Gy).

2. Materials and methods

2.1. Sample preparation, characterization and TL measurements

Both natural monazite from Madagascar and synthetic $CePO_4$:$Nd_{0.20}$,$La_{0.25}$ (prepared by chemical precipitation), were previously characterized by means of X-ray diffraction (XRD), energy disperse spectroscopy (EDS) and cathodoluminescence spectroscopy[7]. The synthetic Nd, Ce-monazite was prepared from the following precursors CeO_2 and Nd_2O_3 that were dissolved in 99% HNO_3 (supplied by J. T Baker). The solutions were added in drops using a peristatic pump into a 0.5 mol/L $(NH_4)_2HPO_4$ solution and a 0.5 mol/L $La(NO_3)_3 \cdot 6H_2O$ solution (J.T Baker 99.9%) in 1:1 molar ratio. The solution was stirred for 1 h at 80 °C at pH=7 added with NH_4OH (J. T. Baker 68%). The solution was then (i) filtered and washed with deionized water at 60 °C until excess ammonia was removed and (ii) dried at 80 °C for 24 h and calcined at 700 °C in air to remove organic matter.

The crystal structure of the natural monazite, similar to the analysis performed on the synthetic sample[7], was examined by XRD, using a Cu Kα (0.15406 nm) radiation at room temperature (RT) on a BRUKER Linxeye XE diffractometer using a step scanning from 10° to 60° 2θ (0.020 steps per second and 0.5 s per step). The obtained result was compared with PDF2 XRD card files from the Joint Committee on Powder Diffraction Standards (JCPDS) using XPowder diffraction software.

The chemical composition was measured by means of energy-dispersive X-ray spectroscopy (EDS) using a Bruker silicon drift detector, coupled to an environmental scanning electron microscope (ESEM), at 30 kV with a detection threshold of 0.01 wt%.

The TL measurements were obtained using an automated Risø system model TL DA-12 where the glow emission was collected by an EMI 9635 QA bialkaline photomultiplier tube through a blue filter (FIB 002 Melles-Griot) with the maximum at 400 nm, transmission in the 320–480 nm range (80(16) FWHM) and peak transmittance over 60%. The glow emissions were obtained at a linear heating rates in the range of 2–8 °C/s from RT to 500 ºC in N_2 atmosphere. The background consisting of both incandescence and detector noise was directly subtracted from the TL data by means of a second TL readout of each of the 8 aliquots for each test (4 corresponding to the mineral sample and 4 to the synthetic one) with a weight of 5.0(1) mg and size of grain of 90 µm. The beta dose was provided using the $^{90}Sr/^{90}Y$ beta source attached in the Risø reader with a dose rate of 0.010 Gy/s calibrated against a ^{137}Cs photon source in a secondary standards laboratory at Ciemat.

2.2. TL kinetic analysis

The TL glow curves were analyzed using both a CGCD program to resolve the individual peaks assuming first order kinetics, and VHR method. The CGCD program fits the glow peaks using a Levenberg–Marquardt algorithm to minimize the χ^2 function (Eq. (1)):

$$\chi^2 = \sum_i \left(I(T_i) - \sum_{n=1}^{\text{Npeaks}} I_n(T_i) \right)^2 \tag{1}$$

Where $I(T_i)$ and $I_n(T_i)$ are the intensities of the measured glow curve and the n^{th} fitting glow peak for temperature T_i, respectively. As a linear heating profile is applied (i.e. $T(t)=T_0+\beta t$), the expression for each glow peak can be written taking into account the kinetic parameters (heating rate β, initial density of trapped charges concentration n_0) using the first order kinetic (FOK) approach, with continuous trap distributions as described in Eq. (2):

$${}^{\text{FOK}}I_n(T) = \frac{s}{\beta} \cdot \int_0^{+\infty} n(E) \cdot \mathrm{e}^{-E/KT} \cdot \exp\left(-\frac{s}{\beta} \int_{T_0}^{T} \mathrm{e}^{-E/KT} \cdot \mathrm{d}T \right) \cdot \mathrm{d}E \tag{2}$$

Where the $n(E)$ corresponds to the density of the trapped charges function related to the Gaussian expression (Eq. (3)):

$$n_{\text{Gauss}}(E) = \frac{n_0}{\sqrt{2\pi\sigma^2}} \cdot \mathrm{e}^{-(E_0-E)^2/2\cdot\sigma^2} \tag{3}$$

Or exponential expression Eq. (4):

$$n_{\mathrm{Exp}} = \frac{n_0}{\sigma} \cdot \mathrm{e}^{-(E-E_0)/\sigma} \tag{4}$$

Eq. (2) is written using the non-geometric parameters (s, β, n_0) where the relationship with the geometric or kinetics parameters (E_0, T_M, I_M, σ) is established taking into account a maximum condition:

$$\left.\frac{\mathrm{d}I(T)}{\mathrm{d}T}\right|_{T=T_\mathrm{M}} = 0 \rightarrow I(T_\mathrm{M}) = I_\mathrm{M} \tag{5}$$

Where T_M and I_M are respectively the temperature and the intensity of the maximum[20]. Then, the following mathematical expression can been obtained:

$$\frac{T_\mathrm{M}^2}{\beta} = \frac{E}{s \cdot k} \exp\left(\frac{E}{k \cdot T_\mathrm{M}}\right) \tag{6}$$

where k is Boltzmann's constant (eV/K), and E is the activation energy (eV). Then, Eq. (2) can be rewritten in terms of their kinetic parameters as follows:

$${}^{\mathrm{FOK}}I_n(T) = I_\mathrm{M} \frac{\int f(E)\, \mathrm{e}^{-\frac{E}{kT}} \exp\left[\frac{-E_0}{kT_\mathrm{M}}\left(\frac{T}{T_\mathrm{M}}\right) \exp\left(\frac{E_0}{kT_\mathrm{M}} - \frac{E}{kT}\right) R\left(\frac{E}{KT}\right)\right] \mathrm{d}E}{\int f(E)\, \mathrm{e}^{-\frac{E}{kT}} \exp\left[\frac{-E_0}{kT_\mathrm{M}} \exp\left(\frac{E_0}{kT_\mathrm{M}} - \frac{E}{kT_\mathrm{N}}\right) R\left(\frac{E}{kT_\mathrm{M}}\right)\right] \mathrm{d}E} \tag{7}$$

It has been considered for the distribution function $n(E)$ that the remaining integral is estimated by means of the Gaussian or Exponential approximation as described in Eqs. (3) and (4)[21], where E_0 is the energy level for the more populate traps and σ corresponds to the parameter describing the width of Gaussian or exponential distribution.

The TL emission was also analysed by VHR method to test the evolution of the TL maxima of 1 Gy-irradiated monazites with heating rates at 2, 3, 4, 6 and 8 ºC/s and, thus, determining both E and s. It has been assumed that the traps are emptied at different heating rates while the rests of the parameters are not modified. As the heating rate is increased, the position of the TL maximum (T_M) is shifted to higher temperature. Heating rate (β) is related to T_M of the peak as expressed in Eq. (6). The resultant plot $\ln(T^2_\mathrm{M}/\beta)$ against $1/(kT_\mathrm{M})$ gives rise to a straight line of slope E/k where the E value does not depend on any other kinetic parameter and the intercept $\ln(E/s \cdot k)$ allows us to estimate the s value. The presence of small satellite peaks surrounding the main maxima has no influence on the calculation of E and s; however, the appearance of several TL overlapping glow peaks does not match with the existing maxima. Therefore, the calculated kinetic parameters using VHR could not correspond to the real values and need to be supported by CGCD method.

3. Results and discussion

3.1. Dose response and linearity

As seen in Fig. 1, the blue TL emission of natural (Fig. 1(a)) and synthetic (Fig. 1(b)) beta irradiated Ce-monazites, previously heated up to 500 °C to remove the charges naturally trapped, differ drastically among them due to the presence of dopants/impurities that are significantly higher in the first sample[7]. The main differences of both samples, which show complex TL curves, consist of: (i) the higher intensity of the natural sample (in a ratio of 8:3) with respect to the synthetic monazite considering the area under the curve in the range of 50–450 ˚C and (ii) the groups of components that, attending to the variation in the slope of the experimental TL glow curve and as a rough estimation, consist of three overlapped maxima at ~90, 130 and 250 ºC for the natural light rare earth elements (LREEs) orthophosphate sample and five maxima peaked at ~90, 180, 230, 280 and 340 ºC for the synthetic Ce-monazite. As will be explained in detail throughout the text, the main differences in the lattice structure and chemical composition of natural and synthetic samples induce changes in the blue TL emission mainly related to the shape of the glow curve.

The enhancement of the glow intensity suggests that the natural sample exhibits an increase of the traps higher than the observed in the synthetic one, where the electron-hole trap centers are associated with 4f and 5f (due to REE^{3+}) → 2p (oxygen) transitions since the sample contains lanthanides (La 4.31%, Ce 11.66%, Nd 4.30%, Sm 0.62%, and Gd 0.35%) and natural actinides (U 0.60% and Th 5.22%) (Fig. 2(a, b)). It is known that a greater presence of impurities in the crystalline structure tends to give rise to a greater possibility of increasing the blue TL intensity that would be mainly associated with structural defects. The monazite structure is flexible enough to incorporate dopants with different radii into the crystal lattice without inducing changes in spatial configuration, allowing co-doping with different lanthanides and actinides. Additionally, it might also be considered that (i) the self-irradiation linked to the presence of Th and U that, according to Meldrum et al.,[22] monazite is not affected by metamictization due to this process, (ii) the presence of paragenetic phases crystallized under physical-chemical conditions similar to those of monazite, namely pretulite, bastnaesite or xenotime (appearing as inclusions in, for instance, pegmatites or alluvial deposits) that can exhibit luminescence[2,24-26] and (iii) the variation in the crystallinity index where the crystallographic structure could be affected by the presence of several types of impurities respect to the synthetic monazite (only Nd and La) that could modify the TL intensity (Fig. 2(c) in this paper and Fig. 1(a) in Ref. 27). Similar XRD results have been reported for natural monazites from Guangxi province,China[28].

The dose response of both samples in the range of 1–8 Gy (insets in Fig. 1) shows a behavior that can be fitted to a linear expression of each component that has been estimated by means of CGCD method. It can be seen how the evolution of the area of each maximum

shows a linear behavior for all of them, although the slope differs among them where the peak at 127 ℃ for the natural sample and 282 ℃ for the synthetic monazite appear as the most intense. Therefore, the dose response exhibits a linear behaviour that is in agreement with the criteria described by Chithambo et al., [29,30] who observed in synthetic $SrAl_2O_4:Eu^{2+},Dy^{3+}$ and natural K-rich feldspar that the growth curve was determined by the super linearity index[29]. Such behavior indicates that (i) there is no saturation for any group of components involved in the TL process; i.e. as the given beta dose increases, the number of charges are hosted in the defects and the traps linked to the intensity of the glow emission are not totally filled and (ii) there is no radiation damage that could lead to ion shift in the lattice or additional electron defects that result in valence state changes of impurities, partial irreversible local phase transitions, etc. inducing changes in spectral emission with increasing the dose. One can observe how the position of the maxima does not modify the position of the temperature with the given dose denoting, therefore, a first-order kinetic luminescence mechanism for both samples[31].

3.2. TL kinetic analysis

3.2.1. Variable heating rate (VHR) method

The calculation of the TL kinetic parameters of the natural and synthetic monazites was performed using both VHR and CGCD methods. As aforementioned, the main lack of VHR appears when the groups of components are nearby giving rise to overlapping maxima leading to inaccuracies in the estimation of the kinetic parameters associated with the luminescent process. Nevertheless, as a reasonable approach, VHR appears as an acceptable solution to determine the *E* and *s* values of isolated peaks. In this regard, the VHR method was applied on the maxima II (~130 ℃) and III (~290 ℃) for the natural monazite and II (~170 ℃) and IV (~275 ℃) for the synthetic material (Fig. 3(a, b)). As appreciated for both samples, the maxima tend to shift the position towards higher temperatures with a decrease of the TL intensity as the heating rate increases. Such displacement of the maxima with higher heating rates would be due to traps emptied later since the charges releasing hosted in the traps are less effective. The behavior of the lower TL intensity maximum of the mineral sample would be associated with a thermal quenching effect (TQE); i.e. decrease in the quantum efficiency of the luminescence emission. However, the maximum peaked at ~90 ℃ corresponding to the synthetic samples displays an anomalous increase in TL intensity with the heating rate. It could be related to a pre-dose effect caused by the simultaneous processes: adsorbed hydroxyl groups, oxygen-vacancy centers, $[H_3O_4]^o$ centers, dehydration of adsorbed water molecules and/or local reversible phase transition of rhabdophane and monazite, although the equilibrium shifts towards the monazite phase, i.e. there is no complete rehydration of the phosphates inducing a low concentration of neo-formed thin rhabdophane layer on the monazite surface by adsorption of environmental H_2O molecules at RT[32,33]. The dehydration of the adsorbed water molecules placed in the first coordination shell of the luminescent ions could induce to oscillating hydroxyl groups that absorb energy giving rise to faster return of

the electrons to their ground state with the consequent emission of photons in the UV-blue region. As observed in Fig. 3(c, d), the Arrhenius plots ln$I$ against $1/(kT_m)$ corresponding respectively to maxima II and III for the natural sample and II and IV for the synthetic phosphate, display straight lines where the E and s kinetic values are shown in Table 1 which are reasonably well correlated with the kinetic parameters assessed by means of CGCD method (Table 2) for the isolated peaks. From the VHR results one can also conclude that both natural and synthetic samples display TQE considering the whole area of the experimental data (Fig. 4 and Table 3). The analysis carried out considering each group of components individually by means of the CGCD technique, indicates that all of them show TQE for the natural sample. However, the synthetic monazite exhibits a mixed behavior where peaks I and III seem to be non-affected by TQE. The largest divergence observed in the TL kinetic parameters corresponding to the maxima peaked at ~130 ℃ (in natural monazite) and ~170 ℃ (in synthetic monazite) denotes the presence of overlapping peaks (Tables 1 and 2).

3.2.2. Computerized glow curve deconvolution (CGCD) method

The estimation of the TL kinetic parameters corresponding to superimposed maxima needs to be determined with a more precise and accuracy method (CGCD) that is supported by the second derivative peak detection (Fig. 5). It rises as a method to resolve overlapping maxima into individual components based on the estimation of the curvature of the TL glow curve that is the rate of the change of the slope of the experimental glow emission without the need to carry out the T_m-T_{stop} test[34]. The negative minima will be associated with the local maximum peak that will give information on the position, height and width of each component. In this sense, the application of the second order derivative analysis performed on the TL glow curves confirms the existence of four and five peaks for the natural and the synthetic monazites respectively (Fig. 5). The TL kinetic parameters were calculated assuming a trap structure following a linear combination of four (for the natural sample) and five (for the synthetic monazite) FOK with exponential continuous distribution functions for the lower temperature peaks and FOK functions with a Gaussian continuous distribution of the charges for the rest groups of components. As illustrated in Fig. 5(a, b), figure of merit (FOM) values are below 3% accurately indicating an acceptable fitting despite the complexity of the curves.

All deconvoluted peaks are associated with the chemical-physical processes that, due to these measurements were performed using a UV-blue filter, would be mostly linked to intrinsic and structural defects as well as chemical reactions. In this sense, one can identify the presence of one maximum at 80–90 ℃ for both samples (mineral and synthetic) whose origin has already been previously explained. The main peak in the natural $CePO_4$ centred at 127 ℃, which does not appear in the synthetic sample, could be related to defects mainly due to the presence of impurities in the orthophosphate lattice that include La^{3+} (ionic radii 0.1216 nm), Nd^{3+} (0.1163 nm), Sm^{3+} (0.1132 nm), Gd^{3+} (0.1107 nm) and natural actinides

(U^{4+} 0.1 nm and Th^{4+} 0.109 nm) which replace Ce^{3+} (0.1196 nm) in the monazite crystalline lattice. Such substitutions, which occur easily due to the flexibility of the Ce-monazite structure to host different dopants as aforementioned, produce (i) structural disordering inducing distortions in the monoclinic lattice of the material giving rise to an increase in the concentration of intrinsic defects and, therefore, variation in the Fermi level that cause modifications in the TL curve and (ii) the local structural transformation of monoclinic into tetragonal xenotime structure due to the presence of U that modifies the space group ($I4_1/amd$) and the coordination as well as the rotation of the PO_4 tetrahedral; U exhibits an eight-fold oxygen coordinated structure. But it is also that this effect is amplified since the cations are not isoelectronic; 3 U(IV) have to replace 4 Ce(III). In this sense, it would be expected that the restructuring of the crystal lattice would induce, among others, the formation of non-bridging oxygen hole centers (NBOHCs) that will act as charge traps favoring the appearance of this TL peak. Both samples display TL emission above 160 ℃, although this differs significantly since the natural sample shows two broad peaks centered at 200 and 272 ℃, whilst in the synthetic monazite one can appreciate the presence of 4 groups of components peaked at 178, 236, 282 and 340 ℃. Nevertheless, this glow emission could be considered similar for both samples where the highly-ordered crystalline lattice of the synthetic sample will allow us to differentiate the physical-chemical processes that take place in the materials and that are revealed by a splitting of the TL signal. Thus, although it is necessary to carry out a more specific study of the assignment of each peak with respect to the physical-chemical process that occurs in both monazites, it could be considered that the TL emission in this UV-blue spectral region could be mainly due to (i) transitions from $4f^05d^1 \rightarrow 4f^1$ ground state ($^2F_{5/2}$ and $^2F_{7/2}$ levels) of Ce^{3+} that shows partially filled 4f shell shielded by $5s^2$ and $5p^6$ orbitals[35,36]. (ii) $Ce^{3+} \leftrightarrows Ce^{4+}$ redox reaction that can be promoted by increasing the temperature due to the TL readout in combination with the given dose (1 Gy) that induces the ionizing effect for this reaction, but is negligible for a potential radiation-induced amorphization effect or any other structural radiation damage[37]. (iii) Loss of O atoms from the PO_4 groups that produce oxygen deficient centers (ODCs) which modify the length of the P–O bond and generate charge traps since the nine-fold oxygen coordinate structure turns into a CeO_8 polyhedral[10]. And, among others, (iv) Frenkel defects (i.e. interstitial vacancies) that can occur during irradiation maintaining charge balance, but inducing a local electronic disorder. These defects stem mainly from the dissociation of oxygen atom from orthophosphate groups, leading to the formation of oxygen ion vacancy-interstitial PO_4^{3-} centers known as a Frenkel pair and, the energy of the formation of these defects could be assessed from the energies of the unit cells derived of the ion positions in the monazite lattice[10]. The shift of Frenkel defects along the crystal lattice is usually related to radiation damage, which is of particular interest for neutron dosimetry purposes where the incidence of the neutron beam can displace atoms in the crystalline lattice of the material causing point defects. The energy transferred to the material by neutrons, known as the Wigner energy, can induce the release of energy abruptly causing an increase in temperature[38]. The changes in the lattice

structure due to the formation of vacancy-interstitial pairs give rise to modifications in the TL properties of the material and, consequently, in the kinetic parameters that lead to the luminescence processes providing information on the atomic structure. The assessment of the TL kinetic parameters using the CGCD method, as well as the estimation of the uncertainties associated with the *E*, *s*, σ and *b* values, are shown in Table 2. Such uncertainty analysis was carried out using the classical GUM guidance considering a confidence limit of 95% accuracy and standard deviation 1σ that is linked to the mean value of each group of 4 aliquots corresponding to both mineral and synthetic samples[39].

Fig. 6 shows a breakdown of the kinetic parameters (*E*, *s* and the electron population $-n_i$-) where, as expected and derived from Eq. (6), the s values will depend on both the trap depth and the T_{max} (position of the intensities of the maxima) when each group of components is deconvoluted (Fig. 6(a, b) and Table 2). The kinetic analysis was carried out assuming FOK exponential distribution for the Peak I for both mineral and synthetic samples and FOK Gaussian distributions for the rest of the maxima. Fig. 6(c , d) show (i) the uncertainties for the estimation of the trap depth corresponding to each group of components (four and five peaks for natural and $CePO_4$:$Nd_{0.20}$,$La_{0.25}$ monazites respectively) and (ii) the distribution of the groups of components according to the n_i which used to be directly proportional to the total radiation absorbed dose. The distribution of the electron population in the traps differs significantly for the peak I (T<120 ^oC) because the kinetics follows an expression based on a FOK with exponential distribution function[40].

4. Conclusions

The study performed on the glow emission of synthetic and natural Ce-monazites shows a potential methodology to identify microscopic defects from a qualitative viewpoint based on the kinetic parameters that lead to the TL process. Both samples exhibit complex TL curves with significant differences in their shape, mainly due to (i) the content of impurities (natural sample contains lanthanides as well as U 0.60% and Th 5.22%) and (ii) the degree of crystallinity of the samples which is directly related to the type of impurities (synthetic monazite relies only on Nd and La).

Nevertheless, both samples show similar behavior with respect to dose response in the range of 1–8 Gy; glow intensity increases linearly as the dose increases without changes in the position of the maxima denoting a first-order kinetic luminescence mechanism. The assessment of the kinetic parameters by means of the CGCD method allows to identify maxima peaked at ~90, 130 and 290 ℃ (for the mineral sample) and ~90, 170, 220, 270 and 320 ℃ (for the synthetic Ce-monazite) with FOM values of the glow curves fitted below 3%. Each peak is linked to chemical-physical processes mostly due to structural defects (i.e. phase transitions), chemical reactions (i.e. $Ce^{3+} \leftrightarrows Ce^{4+}$ redox reaction, dehydration or dehydroxylation processes) or intrinsic defects (i.e. Frenkel defects, ODCs or NBOHCs).

References

1. Ji Y, Kowalski PM, Kegler P, Huittinen N, Marks NA, Vinograd VL et al. Rare-earth orthophosphates from atomistic simulations. *Front Chem*. 2019;7:197.
2. Boatner L. Synthesis, Structure, and Properties of Monazite, Pretulite, and Xenotime. *Rev Mineral Geochem*. 2002;48(1):87. Rev Mineral Geochem.
3. Rao RP, Devine DJ. RE-activated lanthanide phosphate phosphors for PDP applications. *J Lumin*. 2000;87-89:1260.
4. Gallini S, Jurado JR, Colomer MT. Synthesis and characterization of monazite-type Sr:$LaPO_4$ prepared through coprecipitation. *J Eur Ceram Soc*. 2005;25:2003.
5. Kumar V, Singh S, Kotnala RK, Chawla S. $GdPO_4$:Eu^{3+} nanoparticles with intense orange red emission suitable for solar spectrum conversion and their multifunctionality. *J Lumin*. 2014;146:486.
6. Kukreti BM, Kumar P. Developing a correlation index and U disequilibrium factor for the exploratory boreholes in Wahkut block of West Khasi Hills district, Meghalaya (India). *Appl Radiat Isotopes*. 2013;72:6.
7. Barrera-Villatoro A, Boronat C, Rivera-Montalvo T, Correcher V, Garcia-Guinea J, Zarate-Medina J. Cathodoluminescence response of natural and synthetic lanthanide-rich phosphates (Ln^{3+}:Ce,Nd). *Radiat Phy Chem*. 2017;141:271.
8. Chong S, Riley BJ, Nelson ZJ. Crystalline compounds for remediation of rare-earth fission products: A review. *J Rare Earths*. 2022;40(3):365.
9. Ferhi M, Horchani-Naifer K, Férid M. Combustion synthesis and luminescence properties of LaPO4: Eu (5%). *J Rare Earths*. 2009;27(2):182.
10. Yi Y, Zhao XF, Teng YC, Bi B, Wang LL, Wu L et al. First-principles study of point defects in $CePO_4$ monazite. *J Nucl Mater*. 2016;482:170.
11. Mashrur Zaman M, Antao SM. Crystal structure refinements of four monazite samples from different localities. *Minerals.* 2020;10(11):1028.
12. Potanina E, Golovkina L, Orlova A, Nokhrin A, Boldin M, Sakharov N. Lanthanide (Nd, Gd) compounds with garnet and monazite structures. Powders synthesis by "wet" chemistry to sintering ceramics by Spark Plasma Sintering. *J Nucl Mater*. 2016;473:93.
13. Correcher V, Garcia-Guinea J. Cathodo- and photoluminescence emission of a natural Mg-Cr carbonate layered double hydroxide. *Appl Clay Sci*. 2018;161:127.
14. May CE, Partridge JA. Thermoluminescent kinetics of alpha-irradiated alkali halides. *J Chem Phys*. 1964;40:1401.
15. Chen R. On the calculation of activation energies and frequency factors from glow curves. *J Appl Phys*. 1969;40:570.
16. Aramu F, Brovetto P, Rucci A. Activation energy in the NaCl thermoluminescence. *Phys Lett.* 1966;23:308.
17. Topaksu M, Correcher V, Garcia-Guinea J, Yüksel M. Effect of heating rate on the thermoluminescence and thermal properties of natural ulexite. *Appl Radiat Isotopes*. 2015;95:222.

18. Kitis G. TL glow-curve deconvolution functions for various kinetic orders and continuous trap distribution: Acceptance criteria for E and s values. *J Radioanal Nucl Chem*. 2001:247(3);697.
19. Gomez-Ros JM, Furetta C, Correcher V. Simple methods to analyse thermoluminescence glow curves assuming arbitrary recombination-retrapping rates. *Radiat Prot Dosim*. 2006;119:339.
20. Gomez-Ros JM, Correcher V, Garcia-Guinea J, Delgado A. Kinetic parameters of lithium and aluminium doped quartz from thermoluminescence glow curves. *Radiat Prot Dosim*. 2002;100(1-4):399.
21. Correcher V, Gomez-Ros JM, Garcia-Guinea J, Delgado A. Thermoluminescence kinetic parameters of basaltic rock samples due to continuous trap distribution. *Nucl Instr Methods A*. 2004;528(3):717.
22. Meldrum A, Boatner LA, Weber WJ, Ewing RC. Radiation damage in zircon and monazite. *Geochim Cosmochim Acta*. 1998;62(14):2509.
23. Bernhard F, Walter F, Ettinger K, Taucher J, Mereiter K. Pretulite, $ScPO_4$, a new scandium mineral from the Styrian and Lower Austrian lazulite occurrences, Austria, *Am Mineral*. 1998;83(5-6):625.
24. Montel JM, Razafimahatratra D, de Parseval P, Poitrasson F, Moine B, Seydoux-Guillaume AM et al. The giant monazite crystals from Manangotry (Madagascar). *Chem Geol*. 2018;484:36.
25. Imashuku S, Wagatsuma K. X-ray-excited optical luminescence imaging for on-site identification of xenotime. *J Geochem Explor*. 2021;225:106763.
26. Wang H, Li M, Zhang D, Gao K, Li J, Weng Z et al. Phase change, micro-structure and reaction mechanism during high temperature roasting of high grade rare earth concentrate. *J Rare Earths*. 2020;38(10):1140.
27. Roman-Lopez J, Correcher V, Garcia-Guinea J, Rivera T, Lozano IB. Thermal and electron stimulated luminescence of natural bones, commercial hydroxyapatite and collagen. *Spectrochim Acta A*. 2014;120:610.
28. Cao Z, Wu X, Khoso SA, Zhang W, Liu Y, Tian M et al. Effect mechanism of nonane-1,1-bisphosphonic acid as an alternative collector in monazite flotation: Experimental and calculational studies. *J Rare Earths*. 2022;40(5):822.
29. Chithambo ML, Wako AH, Finch AA. Thermoluminescence of $SrAl_2O_4:Eu^{2+}$, Dy^{3+}: Kinetic analysis of a composite-peak. *Radiat. Meas*. 2017;97:1.
30. Kalita JM, Chithambo ML. Phototransferred thermoluminescence characteristics of microcline ($KAlSi_3O_8$) under 470 nm blue- and 870 nm infrared-light illumination. *Appl Radiat Isotopes*. 2022;181: 110070.
31. Alajlani Y, Can N. Thermoluminescence glow curve analysis and kinetic parameters of Dy-doped $BaSi_2O_5$ phosphor. *J Rare Earths*. 2022;40(2):234.
32. Garcia-Guinea J, Garrido F, Lopez-Arce P, Correcher V, de la Figuera J. Spectral green cathodoluminescence emission from surfaces of insulators with metal-hydroxyl bonds. *J Lumin*. 2017;190:128.

33. Arinicheva Y. Monazite-type ceramics as nuclear waste form: crystal structure, microstructure and properties. Energie & Umwelt /Energy & Environment Band/Vol. 459. Forschungszentrum Jülich GmbH, Zentralbibliothek, Verlag. Inst. of Energy and Climate Research. Nuclear Waste Management and Reactor Safety (IEK-6). 2019.
34. Souadi G, Oglakci M, Kaynar UH, Correcher V, Benavente, JF, Bulcar K et al. Thermoluminescence glow curve analysis and kinetic parameters of Eu doped Li_2MoO_4 ceramic phosphors. *Ceram Int*. 2022;48(13):19258.
35. Nuñez NO, Liviano SR, Ocaña M. Citrate mediated synthesis of uniform monazite $LnPO_4$ (Ln=La,Ce) and Ln:$LaPO_4$ (Ln=Eu,Ce,Ce+Tb) spheres and their photoluminescence. *J Coll Interface Sci*. 2010;349(2):484.
36. Takahashi H, Matsushima Y. Luminescent properties of RE-doped mullite ($Al_6Si_2O_{13}$) phosphors (RE=Ce^{3+},Eu^{2+},Ce^{3+}-Tb^{3+}, and Eu^{3+}). *ECS Trans*. 2018;88:237.
37. Kim H, Kim M, Byeon SH. Ce^{4+}/Ce^{3+} redox-controlled luminescence 'off/on' switching of highly oriented $Ce(OH)_2Cl$ and Tb-doped $Ce(OH)_2Cl$ films. *J Mater Chem C*. 2017;5(2):444.
38. Zhao YM, Jin YH, Lv SS, Gao J, Zhou Z, Yano T et al. The Wigner energy and defects evolution of graphite in neutron-irradiation and annealing. *Radiat Phys Chem*. 2022;201:153663.
39. Ainsbury EA, Samaga D, Della Monaca S, Marrale M, Bassinet C, Burbidge CI et al. Uncertainty on radiation doses estimated by biological and retrospective physical methods. *Radiat Prot Dosim*. 2018;178(4):382.
40. Benavente JF, Gomez-Ros JM, Correcher V. Characterization of the thermoluminescence glow curve of $Li_2B_4O_7$:Cu,Ag. *Radiat Meas*. 2020;137:106427.

Journal Pre-proof

Figure Captions

Figure 1. TL glow emission of natural (a) and synthetic (b) monazite with dose in the range of 1–8 Gy. The insets show the evolution of the TL intensity of each component that has been estimated by means of CGCD method.

Figure 2. (a) Environmental scanning electronic microscopy (ESEM) picture of natural monazite grains from Madagascar (100 μm) containing mainly apatite as well as biotite, garnet and bastnaesite among others[23]; (b) EDS chemical analysis of the natural light rare earth element (LREE) phosphate; (c) X-ray diffraction pattern from the natural monazite monocrystal from Madagascar in the 2θ range of 0°–65° (pattern of standard data PDF2 card no. 1.53-70).

Figure 3. 400 nm-TL curves of 1 Gy beta irradiated natural (a) and synthetic (b) Ce-monazite obtained at different heating rates (2–8 °C/s); VHR Arrhenius plots corresponding to the maxima II and III of natural monazite (c) and the groups of components peaked at 160–180 °C (maximum II) and the highest intensity maximum (IV) linked to the synthetic sample (d).

Figure 4. Thermal quenching of natural (a) and synthetic (b) monazite where each dot corresponds to the area under the experimental whole curve (A_T) (i) and the area estimated under each peak (P_i) using the CGCD method (ii). Solid lines are related to the linear fitting obtained in the range of 2–8 °C/s.

Figure 5. UV-blue TL curves fitting of natural (a) and synthetic (b) monazite displaying the experimental data (cross), the fitted curves (solid lines) resulting of the sum of the fitted peaks (dashed lines). The second derivative of the experimental TL data allows determining the local minima at peak positions for the natural (c) and synthetic (d) LREE orthophosphate samples. Note that the FOM values lower than 3%.

Figure 6. Trap structure considering the frequency factor (s in s^{-1}) versus activation energy (E in eV) for natural monazites (a) and synthetic $CePO_4$:$Nd_{0.20}$,$La_{0.25}$ (b). Electron population (n in cm^{-3}) vs E values are shown for natural (c) and synthetic (d) monazites. The uncertainties bars related to trap depth of the center values of each Gaussian distribution and the minimum depths for the exponential ones are added.

Journal Pre-proof

Table 1. TL kinetic parameters obtained from the VHR method for the natural and synthetic samples

	Natural monazite		Synthetic monazite	
	Peak II	Peak III	Peak II	Peak IV
T_{max} (°C)	~130	~290	~170	~275
E (eV)	0.88(6)	1.06(9)	0.70(9)	1.12(9)
s (s^{-1})	6.64×10^{12}	3.56×10^{8}	7.09×10^{7}	8.71×10^{11}

Table 2. Kinetic parameters (activation energy E_0 in eV, pre-exponential factor s in $s^{-1}$and width distribution of the E_0–σ in eV) obtained for 1 Gy-irradiated monazites (natural and synthetic) measured at 5 °C/s using CGCD method considering a mathematical model based on a linear combination of functions related to the FOK approach.

Natural					
Peak	Distribution	T_{max} (°C)	E_0 (eV)	σ (eV)	s (s^{-1})
I	Exp.	83	1.21(9)	0.03(2)	6.88×10^{16}
II	Gaus.	127	1.66(4)	0.05(1)	2.64×10^{20}
III	Gaus.	200	0.8(1)	0.04(1)	4.97×10^{08}
IV	Gaus.	272	1.39(7)	0.06(1)	2.56×10^{12}
Synthetic					
Peak	Distribution	T_{max} (°C)	E_0 (eV)	σ (eV)	S (s^{-1})
I	Exp.	91	1.2(1)	0.04(2)	8.65×10^{16}
II	Gaus.	178	1.11(6)	0.008(8)	8.28×10^{11}
III	Gaus.	236	1.25(8)	0.02(1)	7.67×10^{11}
IV	Gaus.	282	1.32(3)	0.01(1)	1.96×10^{11}
V	Gaus.	339	1.3(1)	0.04(3)	9.64×10^{09}

Journal Pre-proof

Table 3. Thermal quenching fitted to an expression of the sort $y = a + b \cdot x$. The heating rate (β) is an independent variable and the total area (A_T) under the TL curve and the area for each peak (P_i) are dependent variables.

Natural						
FOM	β (°C/s)	A_T	P_I	P_{II}	P_{III}	P_{IV}
2.39%	2	1642250	155548	1154708	134361	189601
2.41%	3	1591965	158392	1156444	121008	175540
2.40%	4	1576773	166912	1162966	104191	170188
2.80%	6	1592734	131141	1166179	108207	163964
3.72%	8	1366099	94573	1122547	78191	109682
a		1730131	191448	1172599	146492	216017
b		–38297	–10899	–4354	–8109	–11787
r^2		0.73	0.80	0.36	0.87	0.86

Synthetic							
FOM	β (°C/s)	A_T	P_I	P_{II}	P_{III}	P_{IV}	P_v
1.82%	2	720658	70544	66547	92407	411515	61895
1.85%	3	689466	67891	68351	103257	382919	60145
1.79%	4	688250	66864	64898	94615	378801	47646
2.29%	6	659796	72736	66847	103200	362565	42690
2.86%	8	648458	74286	63839	114554	319367	43333
a		733142	66053	68215	87385	433778	66736
b		–11264	959	–461	3092	–13640	–3390
r^2		0.92	0.5	0.4	0.7	0.94	0.78

Journal Pre-proof

Journal Pre-proof

Graphical Abstract

TL glow emission of natural (a) and synthetic (b) monazite with dose in the range of 1–8 Gy. The insets show the evolution of the TL intensity of each component estimated by CGCD method.

Journal Pre-proof

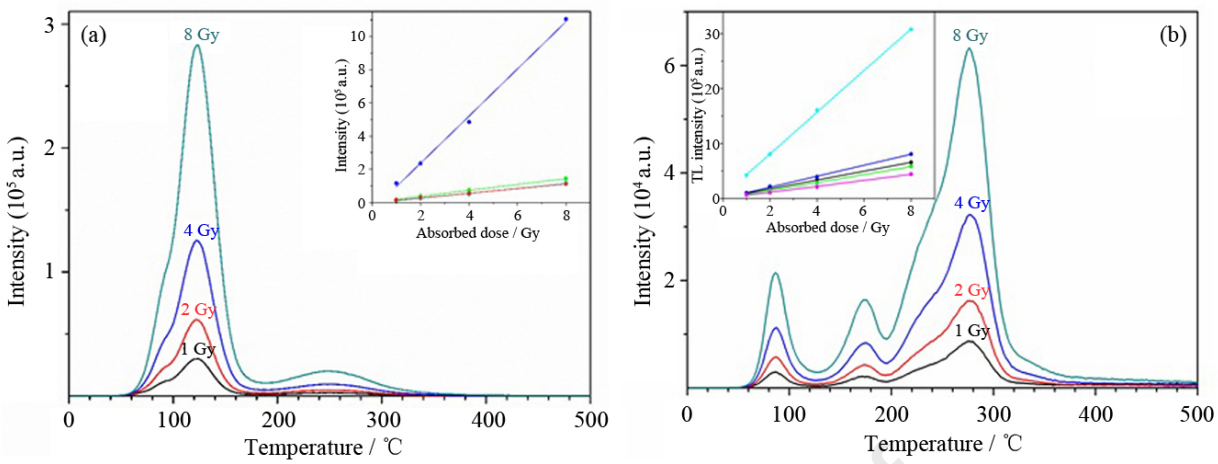

Journal Pre-proof

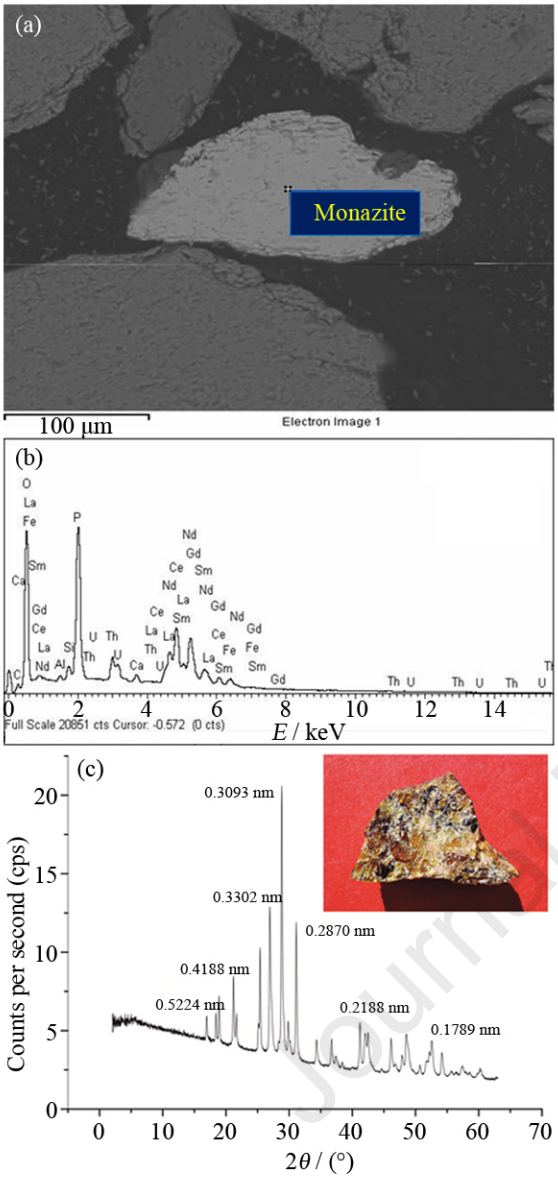

Journal Pre-proof

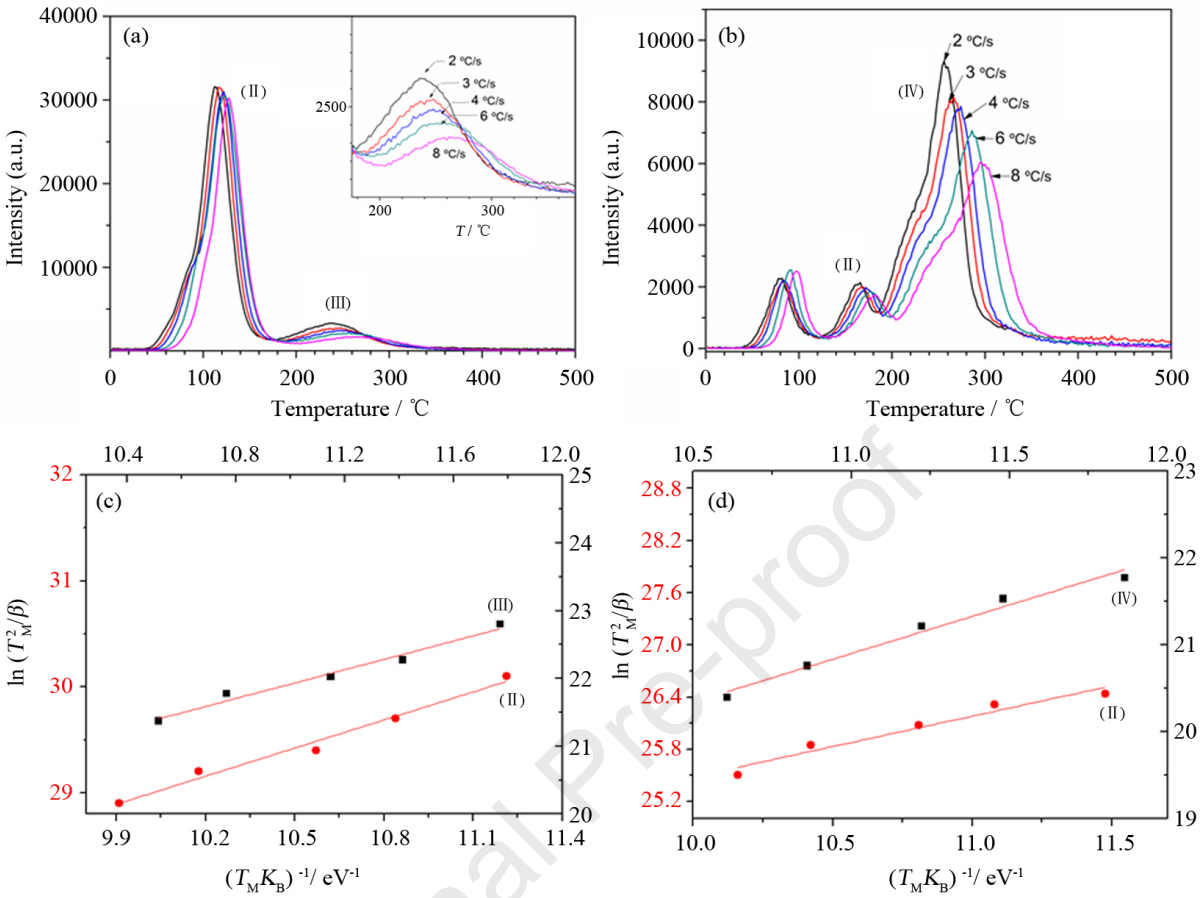

Journal Pre-proof

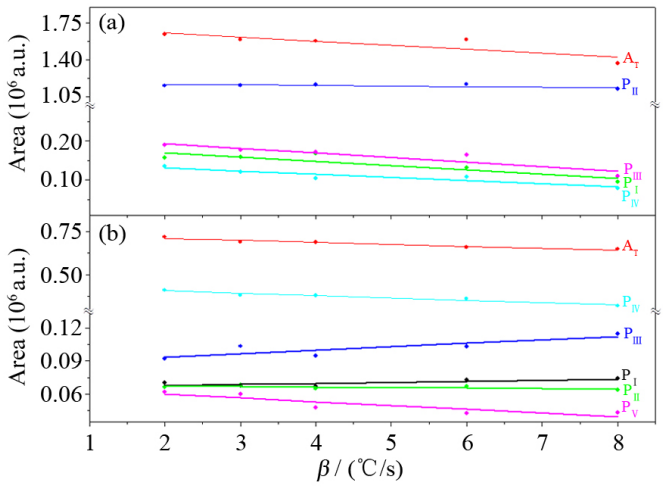

Journal Pre-proof

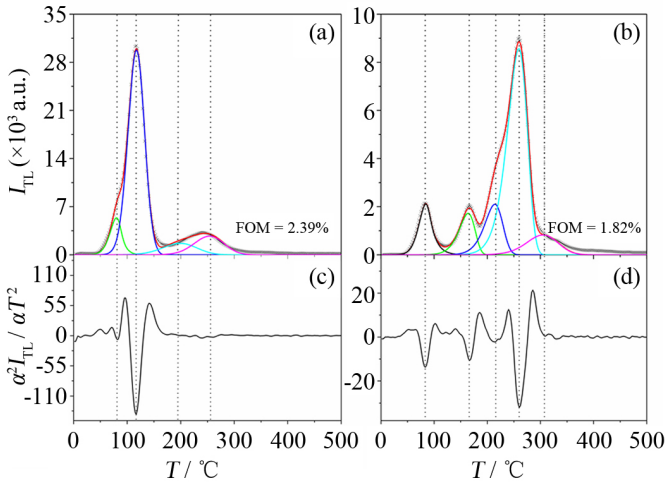

Journal Pre-proof

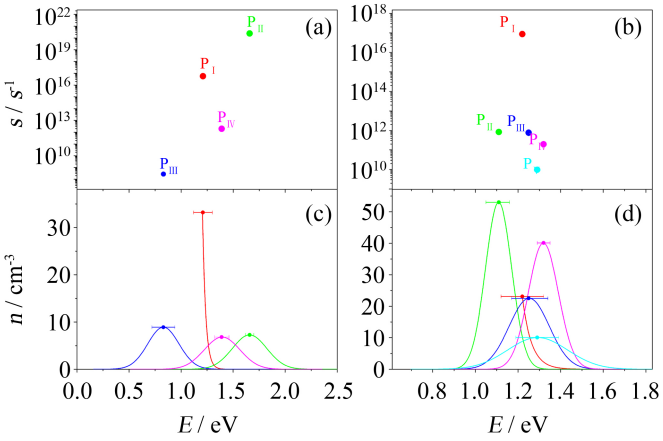

Journal Pre-proof

Journal Pre-proof

Declaration of interests

☒ The authors declare that they have no known competing financial interests or personal relationships that could have appeared to influence the work reported in this paper.

☐ The authors declare the following financial interests/personal relationships which may be considered as potential competing interests:

Journal Pre-proof